Orbital Energy and Spin Flows in a Strong Focus of Laser Light

Victor V. Kotlyar
Anton G. Nalimov
Sergey S. Stafeev
Alexey A. Kovalev
Alexey P. Porfirev
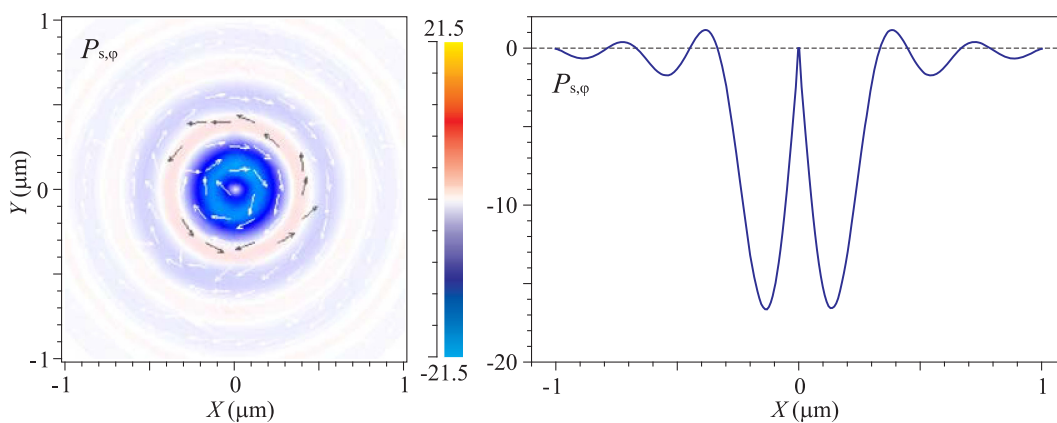
Orbital Energy and Spin Flows in a Strong Focus of Laser Light

Victor V. Kotlyar [1,2] **Anton G. Nalimov** [1,2] **Sergey S. Stafeev** [1,2]
Alexey A. Kovalev [1,2] **and Alexey P. Porfirev** [1,2]

[1]IPSI RAS – Branch of the FSRC "Crystallography and photonics", RAS, Samara 443001, Russia
[2]Samara National Research University, Samara 443086, Russia

Abstract: In this work, we derive analytical relations for all projections of the orbital energy flow and spin flow in the focal plane of a strongly focused left-hand circularly polarized Gaussian beam, also calculating a torque exerted upon a dielectric ellipsoidal microparticle in the focus of the beam and discussing results of an experiment on rotating the microparticle around its center of mass. The on-axis projection of the torque exerted upon the microparticle is found to be negative, i.e., directed oppositely to the beam propagation axis. Such a torque is supposed to induce a clockwise rotation of a non-absorbing dielectric particle around its center of mass. We have been demonstrated that a reverse energy flow occurs in the light field regions where the longitudinal projection of the spin flow is negative and larger in magnitude than the longitudinal projection of the orbital energy flow, which is always positive.

Index Terms: Poynting vector, spin flow, orbital energy flow.

1. Introduction

A number of works [1]–[6] have reported on the appearance of the orbital angular momentum in the strong focus of a conventional circularly polarized Gaussian beam, which was then transferred to a microparticle placed in the focal spot. This phenomenon is related to the spin-to-orbital light momentum conversion. Being devoid of the orbital angular momentum, the original beam only has an on-axis spin vector. Meanwhile, a transverse energy flow is observed in the strong focus, leading to the non-zero longitudinal projection of the orbital angular momentum. Spin-orbit interaction in sharp focus has already been studied in works [1]–[6], but there is no detailed description of SAM and OAM within the Richards-Wolf formalism [7]. The Richards-Wolf theory (RWT) [7], which describes the electromagnetic field near the sharp focus, was generalized for the case of a plane interface near the focus [8]. RWT was also generalized for sharp focusing of cylindrical vector beams [9]. In [10], only the longitudinal components of SAM and OAM were calculated using RWT in the sharp focus of a light field with a topological charge and circular polarization. In [11], using RWT, enhancement of the spin-orbit interaction near the focus was studied in the presence of two

interfaces making a stratified medium. In [12], the spin Hall shift was considered for a Gaussian beam in the sharp focus in the presence of a stratified medium, as in [11]. However, the above papers [8]–[12] do not contain analytical expressions derived within the RWT for all components of the orbital energy flow and of the spin flow, while analysis of such expressions allows determining the energy backflow in the sharp focus. Meanwhile it appears possible to describe the energy and spin flows in the vicinity of the strong focus using findings in Refs. [13]–[17], in which the Poynting vector (the energy flow) is represented as a sum of the orbital energy and spin flows. The spin flow is the curl of the spin vector and, therefore, does not transfer the energy. At the same time, the spin flow and the proper spin vector are both measurable quantities [4], [18].

The most effective approach to the analysis of light fields near the sharp focus is given by the Richards-Wolf theory [7]. It allows closed-form describing of all electromagnetic field components near the focus of an arbitrary light field in the entrance of an aplanatic optical system. The larger is the focal length compared to the wavelength, the more accurate is this method. This method has been successfully applied for theoretical analysis in [1]–[6]. In other works [8]–[12], RWT allowed obtaining other physical quantities in the sharp focus, like energy flow density and spin flow density, orbital angular momentum, and spin angular momentum. Other approximate [19] and exact [20]–[22] methods are also known for describing the electromagnetic field near the sharp focus. Although these methods are exact, the solutions for the electric and magnetic fields components are expressed either via infinite series [20], or via a finite number of bulky terms with special functions [21], [22]. Theoretical analysis of exact solutions of Maxwell's equations in the focus is difficult. In addition, there is a very limited number of known exact solutions of Maxwell equations, while RWT allows obtaining relatively simple closed expressions near the sharp focus for a wide class of initial light fields, such as Gaussian and Bessel-Gaussian beams, light fields with an integer topological charge, light fields with homogeneous (linear, circular, elliptic) and inhomogeneous (azimuthal, radial) polarization. Therefore, we use RWT in this work.

Being characterized only by the on-axis spin vector, a circularly polarized plane wave is able to set into rotation an absorbing spherical microparticle [23] and generate a magnetic field in non-magnetic dispersive media (magnetization effect) [24]. In [25], levitation of low-loss fused quartz spheres in vacuum was demonstrated. The rotation of dielectric microparticles along a circular path in focused laser beams has been studied [11], [26]. In [12], rotation of an absorbing asymmetric microparticle around its center of mass was observed, but the particle was located in the side lobe of the diffraction pattern. Due to the SAM, light field can rotate any absorbing particle and a birefringent particle, including a spherical one [23]. In contrast to [23], our work demonstrates rotation around its center of mass of an asymmetric non-absorbing dielectric microparticle located on the optical axis. Rotation of a weakly absorbing sphere around its axis in the focus of a circularly polarized Gaussian beam was first theoretically shown in [27]. The decomposition of the Poynting vector into the orbital and spin constituents makes it possible to come up with a mechanism behind the generation of a reverse energy flow in the strong focus of laser light [28], [29]. For instance, in Ref. [30], the reverse energy flow (the negative value of the on-axis projection of the Poynting vector) was exclusively associated with the phase (vortex) singularity of the light field. But this is not quite the case as an inverse on-axis energy flow has been shown to occur in the focus of a non-vortex light beam [29]. Relying on the decomposition of the Poynting vector in two constituents corresponding to the orbital energy and spin flows, we offer an interpretation of the reverse energy flow, which has been known in optics for quite long (since 1919 [31], [7]) but has so far failed to obtain the proper interpretation. Energy backflow is a rather universal optical phenomenon that occurs not only in sharp focus, but also in some laser beams like, e.g., vector X-waves [32], nonparaxial Airy beams [33] and fractional Bessel vortex beams [34]. Below, we prove that the reverse energy flow occurs in the optical field regions where the on-axis projection of the spin flow is negative and larger in magnitude than the always positive on-axis projection of the orbital energy flow. The decomposition of the Poynting vector in two constituents [13]–[17] results in the angular momentum also being decomposed into two terms: the orbital and the spin angular momentums [35]. It was shown in [36] (equation (4) in [36]) that when a plane wave with left-hand or right-hand circular polarization diffracts by a dielectric microsphere, the azimuthal SAM component and the

longitudinal component of the Poynting vector in the scattered light are independent of the helicity. However, the behavior of the orbital flow of energy and of the spin flow is not discussed in this work, although it is their ratio that determines the presence of the energy backflow. As was shown in [17] for evanescent waves, the transverse SAM components do not depend on the circular polarization handedness, while the longitudinal SAM component and the transverse component of the spin flow depend on the helicity (equations (8), (9) in [17]). However, comparison of the longitudinal components of the orbital energy flow and of the spin flow (equations (8), (9) in [17]) reveals that in this case there is no reverse energy flow, since $|p_z^O| > |p_z^S|$. In this paper, we show that in the sharp focus of a light field with second-order cylindrical polarization $|p_z^O| < |p_z^S|$ and $p_z^S < 0$, that is, there is reverse energy flow.

In this work, which continues the research reported in Ref. [6], we derive analytical relations for all projections of the orbital and spin flows in the focal plane of a strongly focused left-hand circularly polarized Gaussian beam, also calculating a torque exerted upon a dielectric ellipsoidal microparticle in the focus of the beam and discussing results of an experiment on rotating the microparticle around its center of mass.

2. Poynting Vector (Energy Flow)

A. Bekshaev *et al.* [13], [15], [16] have derived a remarkable result, showing that the Poynting vector **P** (energy flow) can be represented as a sum of two constituents: the orbital energy flow $\mathbf{P}_o$ and the spin flow $\mathbf{P}_s$ [14]:

$$\mathbf{P} = \frac{\mathrm{Re}}{2}\left(\mathbf{E}^* \times \mathbf{H}\right) = \mathbf{P}_o + \mathbf{P}_s, \tag{1}$$

$$\mathbf{P}_o = \frac{\mathrm{Im}}{2k}\left(\mathbf{E}^* \cdot (\nabla \mathbf{E})\right), \quad \mathbf{P}_s = \frac{1}{4k}\left(\nabla \times \mathrm{Im}\left(\mathbf{E}^* \times \mathbf{E}\right)\right), \tag{2}$$

where **E** and **H** are the electric and magnetic vectors of an electromagnetic wave, Re and Im are the real and imaginary parts of the number, $\times$ denotes vector multiplication, and k is the wavenumber of light. Decomposition of the Poynting vector into two terms is obtained if the magnetic field vector **H** from the Maxwell equations for monochromatic light is expressed via the curl of the electric field vector **E**. Such a representation of the energy flow vector **P** (Eq. (1)) will help us to give an interpretation of the reverse energy flow, occurring in the sharp focus under certain conditions, in terms of the orbital energy flow $\mathbf{P}_o$ and the spin flow $\mathbf{P}_s$.

From (2), the spin flow $\mathbf{P}_s$ is seen to be the curl of the spin density vector (spin angular momentum, SAM) **S** [17]:

$$\mathbf{S} = \frac{\mathrm{Im}}{2}\left(\mathbf{E}^* \times \mathbf{E}\right). \tag{3}$$

With the divergence of the curl being zero, the spin flow $\mathbf{P}_s$ does not transfer energy but is still a physically meaningful quantity that can be measured [4], [18]. In dipole approximation, the scattering force $\mathbf{F}_{sc}$ acting upon a Rayleigh particle is proportional to the orbital energy flow $\mathbf{P}_o$ [13]–[15]:

$$\mathbf{F} = \mathbf{F}_g + \mathbf{F}_{sc} = \frac{\mathrm{Re}(\alpha)}{4}\nabla|\mathbf{E}|^2 + \frac{\mathrm{Im}(\alpha)}{2}\mathrm{Im}\left(\mathbf{E}^* \cdot (\nabla \mathbf{E})\right), \tag{4}$$

where $\mathbf{F}_g$ is the gradient force and α is dipole polarizability of the particle. The SAM **S** generates a scattering force exerted upon particles that are characterized by both electric, α, and magnetic, β, dipole polarizabilities [15]:

$$\mathbf{F}_{sc} = -\frac{k^3 \mathrm{Re}(\alpha^*\beta)}{12}\mathrm{Im}\left(\nabla \times \left(\mu^{-1}\mathbf{E}^* \times \mathbf{E} + \varepsilon^{-1}\mathbf{H}^* \times \mathbf{H}\right)\right), \tag{5}$$

where μ and ε are the permeability and permittivity of the particle. Also, note that the total energy flow (i.e., the orbital energy and spin flows) generates a force acting upon a particle with electric

current and specific conductivity σ [14]:

$$\mathbf{F} = \frac{\sigma \, \mathrm{Re}}{2} \left(\mathbf{E}^* \times \mathbf{H} \right). \tag{6}$$

Alongside mechanical forces due to the spin flow, dependent on the spin density vector $\mathbf{S}$ is the moment of force $\mathbf{M}$, acting upon an absorbing particle as (in the dipole approximation) [23]:

$$\mathbf{M} = \mathrm{Im}(\alpha)\mathrm{Im} \left(\mathbf{E}^* \times \mathbf{E} \right). \tag{7}$$

For completeness sake, it is worth noting that the SAM $\mathbf{S}$ in Eq. (3) creates magnetization (generating a magnetic field due to a reverse Faraday effect) in a non-magnetic medium with dispersive refractive index [24], [37].

3. Orbital Energy and Spin Flows in the Cartesian and Cylindrical Coordinates

For later use and with a view of deriving equations in the strong focus, the orbital energy and spin flows (2) need to be written in the Cartesian and cylindrical coordinates. To the best of our knowledge, no such relations in the cylindrical coordinates have been reported in the literature so far.

In the Cartesian system, projections of the orbital energy flow vector are given by

$$P_{o,x} = \frac{\mathrm{Im}}{2k} \left(E_x^* \frac{\partial}{\partial x} E_x + E_y^* \frac{\partial}{\partial x} E_y + E_z^* \frac{\partial}{\partial x} E_z \right),$$

$$P_{o,y} = \frac{\mathrm{Im}}{2k} \left(E_x^* \frac{\partial}{\partial y} E_x + E_y^* \frac{\partial}{\partial y} E_y + E_z^* \frac{\partial}{\partial y} E_z \right),$$

$$P_{o,z} = \frac{\mathrm{Im}}{2k} \left(E_x^* \frac{\partial}{\partial z} E_x + E_y^* \frac{\partial}{\partial z} E_y + E_z^* \frac{\partial}{\partial z} E_z \right). \tag{8}$$

Similarly, projections of the spin flow are given by

$$P_{s,x} = \frac{1}{2k} \left(\frac{\partial}{\partial y} \mathrm{Im} \left(E_x^* E_y \right) + \frac{\partial}{\partial z} \mathrm{Im} \left(E_x^* E_z \right) \right),$$

$$P_{s,y} = \frac{1}{2k} \left(\frac{\partial}{\partial z} \mathrm{Im} \left(E_y^* E_z \right) + \frac{\partial}{\partial x} \mathrm{Im} \left(E_y^* E_x \right) \right),$$

$$P_{s,z} = \frac{1}{2k} \left(\frac{\partial}{\partial x} \mathrm{Im} \left(E_z^* E_x \right) + \frac{\partial}{\partial y} \mathrm{Im} \left(E_z^* E_y \right) \right). \tag{9}$$

For optical systems with cylindrical symmetry, which are used to obtain strongly focused light, it would be more convenient to describe projections of the vectors of electric and magnetic fields and derivatives thereof in the cylindrical coordinates. Below, projections of the vectors of the orbital energy and spin flows, Eqs. (8) and (9), are given in the cylindrical coordinates:

$$P_{o,r} = \frac{\mathrm{Im}}{2k} \left(E_r^* \frac{\partial}{\partial r} E_r + E_\varphi^* \frac{\partial}{\partial r} E_\varphi + E_z^* \frac{\partial}{\partial r} E_z \right),$$

$$P_{o,\varphi} = \frac{\mathrm{Im}}{2kr} \left(E_r^* \frac{\partial}{\partial \varphi} E_r + E_\varphi^* \frac{\partial}{\partial \varphi} E_\varphi + E_z^* \frac{\partial}{\partial \varphi} E_z - E_r^* E_\varphi + E_\varphi^* E_r \right),$$

$$P_{o,z} = \frac{\mathrm{Im}}{2k} \left(E_r^* \frac{\partial}{\partial z} E_r + E_\varphi^* \frac{\partial}{\partial z} E_\varphi + E_z^* \frac{\partial}{\partial z} E_z \right). \tag{10}$$

$$P_{s,r} = \frac{1}{2k} \left(\frac{\partial}{r\partial \varphi} \mathrm{Im} \left(E_r^* E_\varphi \right) + \frac{\partial}{\partial z} \mathrm{Im} \left(E_r^* E_z \right) \right),$$

$$P_{s,\varphi} = \frac{1}{2k}\left(\frac{\partial}{\partial z}\operatorname{Im}\left(E_\varphi^* E_z\right) + \frac{\partial}{\partial r}\operatorname{Im}\left(E_\varphi^* E_r\right)\right),$$

$$P_{s,z} = \frac{1}{2k}\left(\frac{\partial}{\partial r}\operatorname{Im}\left(E_z^* E_r\right) + \frac{\partial}{r\partial\varphi}\operatorname{Im}\left(E_z^* E_\varphi\right) + \frac{\operatorname{Im}\left(E_z^* E_r\right)}{r}\right). \tag{11}$$

4. Orbital Energy and Spin Flows in the Focus

We shall use Eqs. (10) and (11) to calculate the orbital energy and spin flows in the focal plane of a strongly focused left-hand circularly polarized Gaussian beam. Projections of the electric field in the vicinity of the sharp focus from a left-hand circularly polarized, circularly symmetric light field (e.g. a Gaussian beam) in the Cartesian and cylindrical coordinates

$$\begin{pmatrix} E_x \\ E_y \end{pmatrix} = \frac{A(\theta)}{\sqrt{2}}\begin{pmatrix} 1 \\ -i \end{pmatrix}, \quad \begin{pmatrix} E_r \\ E_\varphi \end{pmatrix} = \frac{A(\theta)e^{-i\varphi}}{\sqrt{2}}\begin{pmatrix} 1 \\ -i \end{pmatrix} \tag{12}$$

can be derived based on the Richards-Wolf formalism [7]:

$$E_r(r,\varphi,z) = \frac{-i}{\sqrt{2}}e^{-i\varphi}\left(I_{0,0} + I_{2,2}\right),$$

$$E_\varphi(r,\varphi,z) = \frac{1}{\sqrt{2}}e^{-i\varphi}\left(-I_{0,0} + I_{2,2}\right),$$

$$E_z(r,\varphi,z) = -\sqrt{2}e^{-i\varphi}I_{1,1}, \tag{13}$$

where

$$I_{\nu,\mu} = \left(\frac{\pi f}{\lambda}\right)\int_0^{\theta_0}\sin^{\nu+1}\left(\frac{\theta}{2}\right)\cos^{3-\nu}\left(\frac{\theta}{2}\right)\cos^{1/2}(\theta)A(\theta)e^{ikz\cos\theta}J_\mu(x)d\theta, \tag{14}$$

where λ is the wavelength, f is the focal length of an aplanatic system, $x = kr\sin\theta$, $J_\mu(x)$ is the Bessel function of the first kind, and $NA = \sin\theta_0$ is the numerical aperture. The input function amplitude $A(\theta)$ may be chosen in the form of a Bessel-Gaussian function

$$A(\theta) = J_1\left(\frac{2\gamma\sin\theta}{\sin\theta_0}\right)\exp\left(\frac{-\gamma^2\sin^2\theta}{\sin^2\theta_0}\right) \tag{15}$$

where γ is the ratio of the aplanatic system pupil radius to that of the Gaussian beam waist. Expressing the light field components based on Eq. (13), explicit expressions for the constituents of the Poynting vector (energy flow), orbital energy and spin flows in the focal plane ($z = 0$) can be derived in the cylindrical coordinates:

$$P_{o,\varphi} = -\frac{1}{kr}\left(I_{1,1}^2 + I_{2,2}^2\right),$$

$$P_{s,\varphi} = \frac{1}{kr}\left(I_{1,1}^2 + I_{2,2}^2\right) - I_{1,1}\left(I_{0,0} + I_{2,2}\right),$$

$$P_\varphi = -I_{1,1}\left(I_{0,0} + I_{2,2}\right), \quad P_\varphi = P_{o,\varphi} + P_{s,\varphi}, \tag{16}$$

$$P_{o,z} = \frac{1}{2}\left(I_{0,0}\tilde{I}_{0,0} + I_{2,2}\tilde{I}_{2,2} + 2I_{1,1}\tilde{I}_{1,1}\right),$$

$$P_{s,z} = \left(I_{0,0}^2 - I_{2,2}^2\right) - \frac{1}{2}\left(I_{0,0}\tilde{I}_{0,0} + I_{2,2}\tilde{I}_{2,2} + 2I_{1,1}\tilde{I}_{1,1}\right),$$

$$P_z = \left(I_{0,0}^2 - I_{2,2}^2\right), \quad P_z = P_{o,z} + P_{s,z}, \tag{17}$$
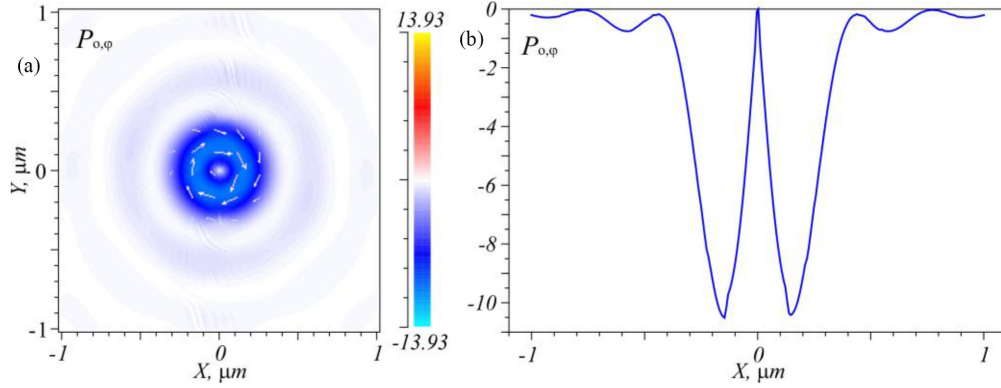
Fig. 1. (a) Distribution of the azimuthal component of the orbital energy flow, $P_{o,\varphi}$ in the focus and (b) its profile along the X-axis.

where

$$\tilde{I}_{\nu,\mu} = \left(\frac{\pi f}{\lambda}\right)\int_0^{\theta_0} \sin^{\nu+1}\left(\frac{\theta}{2}\right)\cos^{3-\nu}\left(\frac{\theta}{2}\right)\cos^{3/2}(\theta)A(\theta)e^{ikz\cos\theta}J_\mu(x)d\theta. \quad (18)$$

In this case, the radial components equal zero: $P_{o,r} = P_{s,r} = P_r = 0$. For completeness sake, the intensity distribution I in the focus for field (12) can be given:

$$I = I_{0,0}^2 + I_{2,2}^2 + 2I_{1,1}^2. \quad (19)$$

From Eq. (17) it is seen that in the focal plane there is a positive orbital energy flow $P_{o,z}$, which is "pushing" a microparticle placed on the optical axis in the positive direction, according to (4).

From (16), it can be seen that when strongly focusing the left-hand circularly polarized Gaussian beam (12), an azimuthal energy flow occurs in the focal plane

$$P_\varphi = -I_{1,1}(I_{0,0} + I_{2,2}) < 0 \quad (20)$$

The near-axis energy flow is negative, rotating clockwise in a similar way to the rotation of the left-hand circularly polarization vector. This energy flow (20) is composed of the orbital energy flow and spin flow (16). Hence, we can infer that when put in the focal plane of the beam, a (non-absorbing) dielectric microparticle, with its center of mass found on the optical axis, will rotate clockwise, according to (4). Presence of the azimuthal component in the orbital energy flow:

$$P_{o,\varphi} = -\frac{1}{kr}\left(I_{1,1}^2 + I_{2,2}^2\right) < 0 \quad (21)$$

implies that the light field in the focus carries a non-zero orbital angular momentum (OAM). Hence, a dielectric microparticle with complex refractive index and its center of mass found on the optical axis in the focal plane will experience the action of two torques, setting it into a clockwise rotation, namely, the on-axis projection of the SAM:

$$S_z = \frac{\text{Im}}{2}(\mathbf{E}^* \times \mathbf{E}) = -\frac{1}{2}\left(I_{0,0}^2 - I_{2,2}^2\right) < 0. \quad (22)$$

and the orbital energy flow in Eq. (21). In the meantime, SAM (22) is able to rotate only an absorbing particle [23], having no impact on a spherical non-absorbing dielectric particle. According to Eq. (22), SAM on the optical axis not zero and negative near the optical axis. This spin angular momentum rotates a dielectric ellipsoidal microparticle around the optical axis and around its center of mass. Our work confirms this both numerically (Fig. 4) and experimentally (Fig. 5). Similarly, in [38] rotation of a birefringent microparticle in an elliptically polarized light beam was demonstrated.
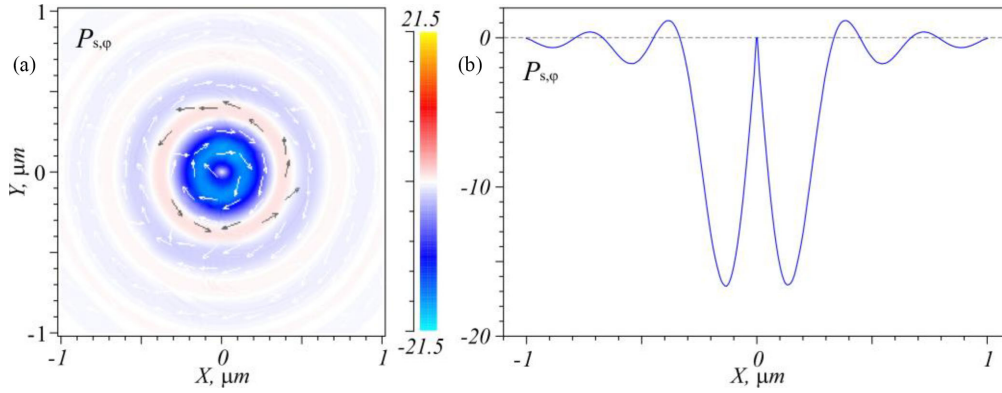
Fig. 2. (a) Distribution of the azimuthal component of the spin flow, $P_{s,\varphi}$ in the focus and (b) its profile along the X-axis.
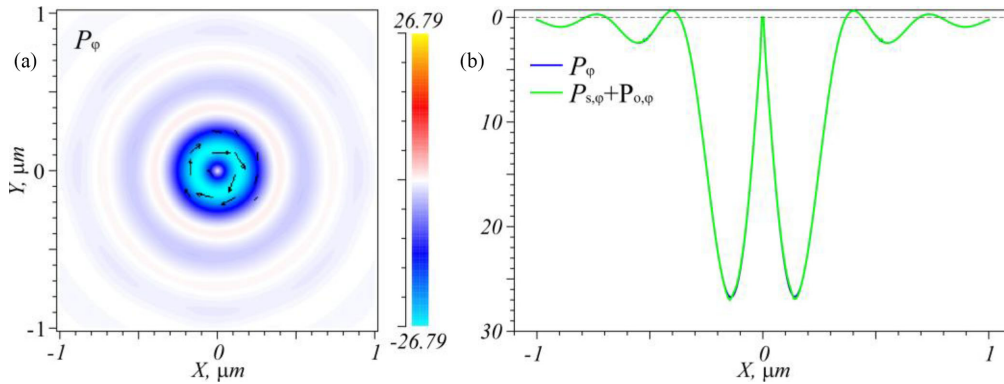
Fig. 3. (a) Distribution of the azimuthal component of the energy flow, P_φ and (b) its profile along the X-axis.

For rotation of a birefringent particle, spin-orbit interaction is not required, only the spin is sufficient (see equation (3) in [38]).

Just as the Poynting vector is the sum of the spin and orbital energy flows, Eq. (1), the angular momentum vector **J** is the sum of OAM, **L** and SAM, **S** [39]–[42]:

$$\mathbf{J} = (\mathbf{r} \times \mathbf{P}) = (\mathbf{r} \times \mathbf{P}_o) + (\mathbf{r} \times \mathbf{P}_s) = \mathbf{L} + \mathbf{S} \tag{23}$$

In view of Eqs. (20), (22) and (23), the on-axis projection of the angular momentum and of OAM in the focus for the field of Eq. (13) reads as

$$J_z = rP_\varphi = -rI_{1,1}\left(I_{0,0} + I_{2,2}\right) < 0 \tag{24}$$

$$L_z = J_z - S_z = -rI_{1,1}\left(I_{0,0} + I_{2,2}\right) + \frac{1}{2}\left(I_{0,0}^2 - I_{2,2}^2\right).$$

On the optical axis, OAM L_z (24) and SAM S_z (22) are identical in magnitude ($I_{0,0}^2/2$) but opposite in sign, therefore, the angular momentum J_z (24) on the optical axis is zero, and the angular momentum near the optical axis is negative. This is also confirmed by the simulation in Fig. 3.
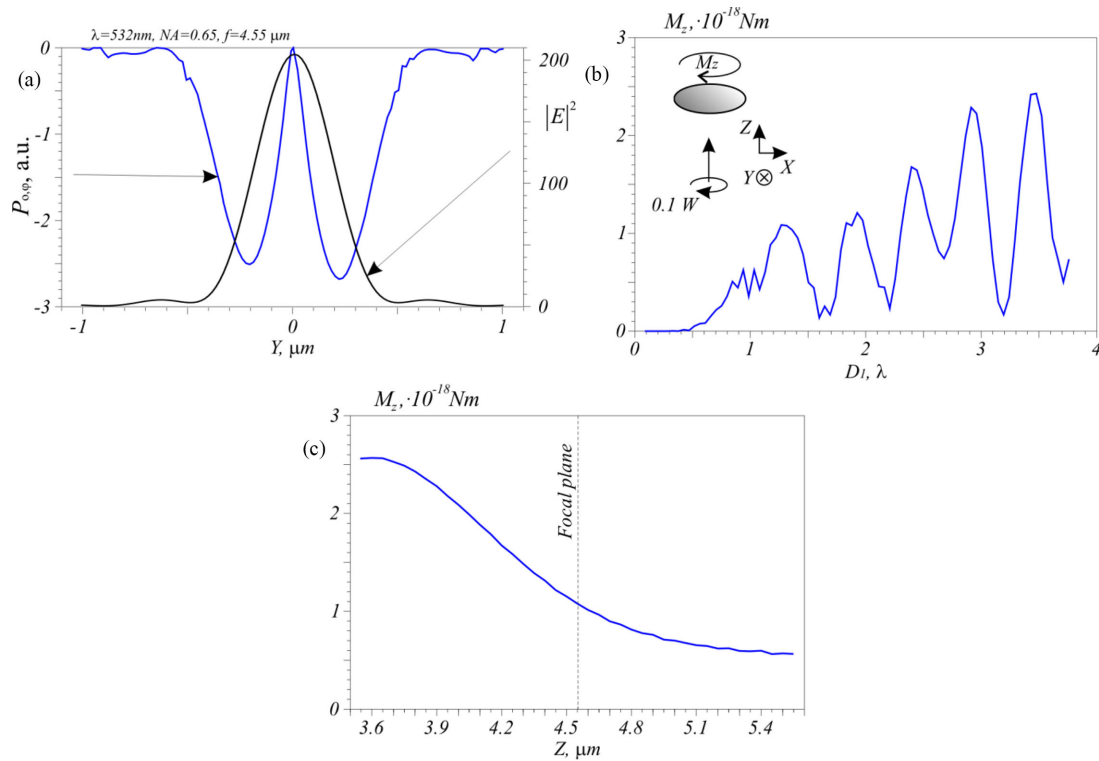
Fig. 4. (a) Radial profiles on the intensity $|E|^2$ and azimuthal component of the orbital energy flow $P_{0,\varphi}$ in the focus (NA = 0.65) of a left-hand circularly polarized Gaussian beam (29); (b) the on-axis projection of the torque M_z versus the larger diameter D_1 of an ellipsoid particle put in the focus of a converging left-hand circularly polarized spherical wave of diameter 8 μm and (c) dependence of the torque Mz on the position of the particle along the optical axis at $D_1 = 1.9\lambda$.
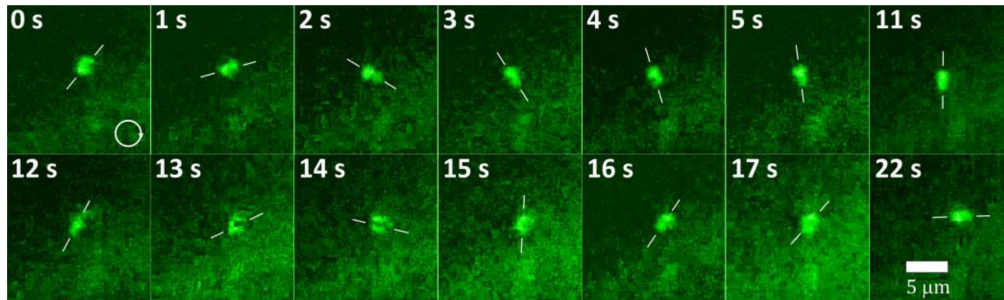
Fig. 5. Rotation stages of a microparticle trapped in a strongly focused left-hand polarized Gaussian beam. The marker lines indicate the orientation of the 2 × 1-μm particle. The marker size is 5 μm.

5. Reverse Energy Flow in the Strong Focus

In this section, we show that the reverse on-axis energy flow is observed in the focus of a light field with the second-order cylindrical polarization reported in Ref. [29] when the on-axis spin flow is negative and larger in magnitude than the positive on-axis orbital energy flow. Let now the initial light field be the following [29] instead of that given in Eq. (12):

$$\begin{pmatrix} E_x \\ E_y \end{pmatrix} = A(\theta) \begin{pmatrix} -\sin 2\varphi \\ \cos 2\varphi \end{pmatrix}, \quad \begin{pmatrix} H_x \\ H_y \end{pmatrix} = A(\theta) \begin{pmatrix} -\cos 2\varphi \\ -\sin 2\varphi \end{pmatrix} \tag{25}$$

Then, projections of the electric and magnetic field in the focal plane are given by

$$H_r(r, \varphi, z) = -i \cos \varphi \, (I_{0,2} + I_{2,0}),$$
$$H_\varphi(r, \varphi, z) = -i \sin \varphi \, (I_{0,2} - I_{2,0}),$$
$$H_z(r, \varphi, z) = 2 \cos \varphi I_{1,1}. \tag{26}$$

Equations (2) and (3) can be represented in a form with 'electric-magnetic democracy' [5], [14]:

$$\mathbf{P}_o = \frac{\mathrm{Im}}{2k}\left(\mathbf{E}^* \cdot (\nabla \mathbf{E}) + \mathbf{H}^* \cdot (\nabla \mathbf{H})\right),$$

$$\mathbf{P}_s = \frac{1}{4k}\left(\nabla \times \left(\mathrm{Im}\left(\mathbf{E}^* \times \mathbf{E}\right) + \mathrm{Im}\left(\mathbf{H}^* \times \mathbf{H}\right)\right)\right). \tag{27}$$

For the light field (26) in the focal plane ($z = 0$), the on-axis projections of the Poynting vector, the orbital energy and spin flows take the form:

$$P_{o,z} = \left(I_{0,2}\tilde{I}_{0,2} + I_{2,0}\tilde{I}_{2,0} + 2I_{1,1}\tilde{I}_{1,1}\right),$$
$$P_{s,z} = \left(I_{0,2}^2 - I_{2,0}^2\right) - \left(I_{0,2}\tilde{I}_{0,2} + I_{2,0}\tilde{I}_{2,0} + 2I_{1,1}\tilde{I}_{1,1}\right),$$
$$P_z = \left(I_{0,2}^2 - I_{2,0}^2\right), \quad P_z = P_{o,z} + P_{s,z}. \tag{28}$$

From (28) it is seen that on the optical axis ($r = 0$), $P_{o,z}(r = 0) = I_{2,0}\tilde{I}_{2,0} > 0$, $P_{s,z}(r = 0) = -(I_{2,0}^2 + I_{2,0}\tilde{I}_{2,0}) < 0$, $|P_{s,z}| > P_{o,z}$, $P_z(r = 0) = -I_{2,0}^2 < 0$. Therefore, the reverse energy flow (negative on-axis projection of the Poynting vector) in the focus [28], [29] is generated because the on-axis projection of the spin flow is negative and larger in magnitude than the positive on-axis projection of the vector of the orbital energy flow. Because of this, contrary to the previously expressed guess, a dielectric microparticle put in the region of the reverse flow will not move in the negative direction [42].

6. Calculating the Orbital Energy and Spin Flows in the Focus

The FDTD-aided numerical simulation using the Fullwave software was conducted for the incident left-hand circularly polarized Gaussian beam of wavelength $\lambda = 633$ nm, with its amplitude multiplied by the transmittance of a thin spherical lens of focal length $f = \lambda$. The transverse components of the original electric field were in the form:

$$E_x = e^{-\frac{r^2}{w^2}} \exp\left(i\left(-kf - \omega t\right)\right), E_y = e^{-\frac{r^2}{w^2}} \exp\left(i\left(-kf - \omega t + \frac{\pi}{2}\right)\right) \tag{29}$$

where $w = 4$ μm, ω is an angular frequency. The focal plane was observed at $z = 600$ nm (somewhat closer than the calculated focal length of $f = \lambda = 633$ nm). The incident field passed through an 8-μm aperture and the simulation was conducted with a $\lambda/30$ increment on all three axes. Fig. 1 depicts (a) the distribution of the azimuthal component of the orbital energy flow, $P_{o,\varphi}$ in the focal plane of field (29) and (b) its radial profile. In the focal plane, the energy is seen to rotate clockwise and, therefore, be negative because the azimuthal angle increases anticlockwise. Fig. 2 depicts (a) the distribution of the azimuthal component of the spin flow, $P_{s,\varphi}$ in the focal plane of field (29) and (b) its radial profile. In the focal plane, the spin vector is seen to rotate clockwise – like the left-hand circularly polarization vector does. Calculations for Figs. 1 and 2 were made using expressions (8) and (9), then results were converted into polar coordinate system taking into account, that $P_{i,\varphi} = -P_{i,x} \sin \varphi + P_{i,y} \cos \varphi$, where $i = o,s$. When summed up, the azimuthal orbital energy flow and spin flow produce the azimuthal component of the Poynting vector, as shown in Fig. 3.

7. Numerical Simulation of the Rotation of a Dielectric Microparticle in the Strong Focus

In this section, we analyze a non-Rayleigh microparticle, which does not satisfy the dipole approximation because it is comparable in size with the incident wavelength and essentially affects the ambient field. Hence, to derive the force and torque exerted upon this particle by the light field we need to rely on a vector theory of diffraction and calculate the Maxwell stress tensor of the electromagnetic field [43], [44].

Let an arbitrary coherent light field falls onto an arbitrary micro particle with a permittivity of ε_1 in a medium with a permittivity of ε_0 (we assume it is equal to 1). Then the torque **M** acting from light on the micro particle relative to an arbitrary point A appear and will be equal [43], [44]:

$$\mathbf{M} = \oint_S [\mathbf{r} \times (\sigma \cdot \mathbf{n})]\, dS \tag{30}$$

where **r** – is the radius-vector from the point A(x, y, z) to a point of integration on the surface S, **n** – is an external normal vector to the surface S, A is the point relative to which the torque **M** is calculated, σ – Maxwell-Minkowski stress tensor, the components of which in CGS system can be written as [45]:

$$\sigma_{ik} = \frac{1}{4\pi}\left(\frac{|\mathbf{E}|^2 + |\mathbf{H}|^2}{2}\delta_{ik} - E_i E_k - H_i H_k\right) \tag{31}$$

where E_i, H_i - electric and magnetic fields components, δ_{ik} - Kronecker symbol ($\delta_{i=k} = 1$, $\delta_{i\neq k} = 0$).

We note that there have been several different definitions of a stress tensor, including those proposed by Abraham, Minkowski and others [46]. For the present purposes, we employ the Minkowski definition (31), because in free space all definitions of the stress tensor [46] are equivalent. The surface S where the torque **M** (30) is calculated is found in free space and chosen so that it envelops the microparticle of interest. The difference between the Minkowski and Abraham stress sensors is insignificant in linear and isotropic materials [46]. Another benefit is that Minkowski stress tensor adequately describes Ashkin's experiments [47], [48] and 2D optical trapping of a polystyrene bead (Fig. 15 [46]).

Fig. 4(b) shows in which way the on-axis projection of the torque M_z, which results in the rotation of an ellipsoidal particle with the ratio of diameters $D_2 = D_1/2$, depends on the larger diameter D_1. For the readers' convenience, Fig. 4(a) depicts (a) the intensity profile $|E|^2$ in the focus of a left-hand circularly polarized Gaussian beam at NA = 0.65 and (b) the radial profile of the azimuthal projection of the orbital energy flow vector $P_{0,\varphi}$ in the focus. The particle's center of mass lies on the optical axis. If it moves from the focal plane along it, the sign of the M_z remains the same (Fig. 4(c)), but it can be seen, that the torque is bigger when the particle is closer to the lens. With the major axis of the ellipse being perpendicular to the optical axis, the torque is calculated relative to the center of mass.

The particle is assumed to be illuminated by a left-hand circularly polarized spherical wave ($r = 6.06\ \mu$m):

$$E_x = \exp\left(i\left(-kr + \frac{\pi}{2} - \omega t\right)\right), E_y = \exp(i\left(-kr - \omega t\right)) \tag{32}$$

passing through a circular aperture of $d = 8\ \mu$m with a focal length of $f = 4.55\ \mu$m (NA = 0.65). The incident wavelength is $\lambda = 532$ nm (power is 100 mW), a microparticle with refractive index $n = 1.5$ is found in the air ($n_0 = 1$), the FDTD-aided numerical simulation is conducted using the Fullwave software with a $\lambda/50$ increment on all three axes. Fig. 4 suggests that with every half-wavelength of diameter increase, there occurs a maximum of the torque M_z, with its minimum being an order of magnitude smaller. The torque and orbital angular momentum (21) have the same direction. Thus, the particle of interest rotates clockwise about its center of mass, i.e., similar to the clockwise rotation of the electric field vector of the incident beam.

Following the work [38], we estimate the torque M_z needed for rotation of an ellipsoid particle in water with the angular velocity $\Omega = 2\pi/6$ (rad/sec), as in our experiment (Fig. 5). To do this, we use the formula $M_z = D\Omega$ with D being the drag torque coefficient which can be estimated for the ellipsoid between the values D for a sphere with a radius a ($D = 8\pi\mu a^3$) and for a disk with the same radius a ($D = 32\mu a^3/3$). So, we suppose for the ellipsoid that $D = 20\mu a^3$. At the room temperature, viscosity of water is $\mu = 0.00091$(Ns/m^2). For our 2×1 μm particle we suppose $a = 1.8 \cdot 10^{-6}$ (m). Thus, we get $M_z = 20 \cdot 0.00091$(Ns/m) $(1.8)^3 \cdot 10^{-18}$(m^3) $\cdot 2\pi/6$(rad/s) $= 0.1 \cdot 10^{-18}$(Nm), whereas, according to Fig. 4, torque for a similar particle in vacuum is an order of magnitude higher: $M_z = 1 \cdot 10^{-18}$(Nm).

8. An Experiment on Rotating a Dielectric Microparticle in the Strong Focus

In the experiment, the original linearly polarized Gaussian beam generated by a solid-state laser ($\lambda = 532$ nm, 100-mW power) was converted into a left-hand circularly polarized beam by passing it through a quarter-wave plate before going to the input pupil of microlens (40×, NA = 0.65) and being focused into a water cell containing polystyrene particles. As a result, the microparticles were being pushed by radiation toward the upper surface of the water cell. The focal length of the microlense was 4.5 mm and the diameter of the focal spot at half-maximum intensity was approximately FWHM = 0.5λ/NA = 0.77λ = 0.41μm. The second microlens (40×, NA = 0.65) imaged the plane of interest onto the video camera array. Results of the experiment on rotating an ellipsoidal type particle approximately measuring 2 x 1 μm in a left-hand circularly polarized Gaussian beam are shown in Fig. 5.

From Fig. 5, the microparticle in the focus of a left-hand circularly polarized beam is seen to rotate clockwise in compliance with Eqs. (20) and (21) and results of the rigorous numerical simulation (Fig. 4). Interestingly, while the size of the microparticles used in the experiment was initially chosen at random, it turned out to be optimal as a local maximum occured at this size (see Fig. 4(b)).

For an absorbing microparticle, the rotation frequency would be several times higher than that measured in the experiment ($\Omega \approx 1$ rad/sec). By way of illustration, the relationship derived in Ref. [23] for a spherical Rayleigh particle gives a rotation frequency of $\omega = IM_gM'M'' \left(\eta c(M'^2 + 2)\right) = 5$ rad/sec, where $M' = $ Re$(n) = 1.6$, $M'' = $ Im$(n) = 0.002$, I is the intensity of light (W/m^2), M_g is the refractive index of the medium (for water, $M_g = 1.33$), and c is the velocity of light in vacuum. This is an overestimated value for the rotation frequency, because the relationship is valid for the Rayleigh particles whose radius is much less than the incident wavelength. This is approximately the same frequency at which strongly absorbing particles would have rotated when trapped in the beam. For example, a 2-μm CuO particle has been described to rotate with a 4-Hz frequency along a circular path in kerosene ($\eta = 1,58 \cdot 10^{-3}$ Ns/m^2) when trapped in a 10-mW beam [49].

We give the following interpretation to rotation of a nonabsorbing dielectric ellipsoidal-type microparticle (Fig. 5). When such a particle is located on the optical axis with its long axis lying in the focal plane, it is rotated around the center of mass and around the optical axis by the orbital energy flow $P_{o,\varphi}$ (21) or, in other words, by the longitudinal OAM component L_z (24), similarly to rotation of particles along a circular trajectory in [11], [26]. Since the effective refractive indices of an ellipsoidal-type particle differ for orthogonal polarizations directed along the long and short axes of the quasi-ellipse (birefringence), it is also rotated around the center of mass by the longitudinal SAM component S_z (22) or, in other words, by the azimuthal spin flow $P_{s,\varphi}$ (16), similarly to rotation of crystalline birefringent particles in [38].

9. Conclusion

Summing up, we have shown theoretically, numerically, and experimentally that the clockwise rotation of a dielectric microparticle in the strong focus of a left-hand circularly polarized Gaussian beam is caused by an azimuthal energy flow or on-axis component of the orbital angular momentum generated in the strong focus due to spin-to-orbital conversion. Previously, a number

of researchers discussed this topic, however a rigorous theory relying upon the Richards-Wolf formalism has not been proposed. The on-axis projection of the torque (derived outside the dipole approximation) exerted upon an arbitrary microparticle whose center of mass lies on the optical axis, has been calculated via the rigorous calculation of diffraction using a Maxwell-Minkowski stress tensor of the electromagnetic field. The direction of the on-axis torque exerted upon the microparticle has been found to be negative relative to the beam propagation axis. This torque should rotate a non-absorbing microparticle clockwise relative to its center of mass. An experiment with an ellipsoidal type 2×1-μm polystyrene microparticle put in the focus of a left-hand circularly polarized Gaussian beam (NA = 0.65, 532-nm wavelength, and 100-mW power) has shown the particle also to rotate clockwise. In addition, we have deduced exact analytical relationships to describe all projections of the orbital energy and spin flows in the focal plane of a strongly focused left-hand circularly polarized Gaussian beam. Based on the deduced equations for the orbital and spin flows in the focus of a light field with second-order cylindrical polarization, the reverse energy flow has been shown to occur in the light field regions where the on-axis projection of the spin flow is negative and larger in magnitude than the always positive on-axis projection of the orbital energy flow.

References

[1] C. Schwartz and A. Dogariu, "Conversation of angular momentum of light in single scattering," *Opt. Express*, vol. 14, no. 18, pp. 8425–8433, 2006.

[2] T. A. Nieminen, A. B. Stilgoe, N. R. Heckenberg, and N. Rubinsztein-Dunlop, "Angular momentum of a strongly focused Gaussian beam," *J. Opt. A*, vol. 10, 2008, Art. no. 115005.

[3] D. Haefner, S. Sukhov, and A. Dogariu, "Spin Hall effect of light in spherical geometry," *Phys. Rev. Lett.*, vol. 102, 2009, Art. no. 123903.

[4] O. S. Rodriguez-Herrera, D. Lara, K. Y. Bliokh, E. A. Ostrovskaya, and C. Dainty, "Optical nanoprobing via spin-orbit interaction of light," *Phys. Rev. Lett.*, vol. 104, Art. no. 253601, 2010.

[5] A. Bekshaev, K. Y. Bliokh, and M. Soskin, "Internal flows and energy circulation in light beams," *J. Opt.*, vol. 13, 2011, Art. no. 053001.

[6] V. V. Koltyar, A. G. Nalimov, and S. S. Stafeev, "Exploiting the circular polarization of light to obtain a spiral energy flow at the subwavelength focus," *J. Opt. Soc. Am. B.*, vol. 36, no. 10, pp. 2850–2855, 2019.

[7] B. Richards and E. Wolf, "Electromagnetic diffraction in optical systems. II. Structure of the image field in an aplanatic system," *Proc. R. Soc. London Ser. A*, vol. 253, pp. 358–379, 1959.

[8] P. Torok, P. Varga, and G. R. Booker, "Electromagnetic diffraction of light focused through a planar interface between materials of mismatched refractive indices: Structure of the electromagnetic field. I.," *J Opt. Soc. Am. A*, vol. 12, pp. 2136–2144, 1995.

[9] Z. Bomzon and M. Gu, "Space-variant geometrical phases in focused cylindrical light beams," vol. 32, no. 20, pp. 3017–3019, 2007.

[10] K. Y. Bliokh, E. A. Ostrovskaya, M. A. Alonso, O. G. Rodriguez-Herrera, D. Lara, and C. Dainty, "Spin-to-orbital angular momentum conversion in focusing, scattering, and imaging systems," *Opt. Express*, vol. 19, no. 27, pp. 26132–26149, 2011.

[11] B. Roy, N. Ghosh, S. D. Gupta, P. K. Panigrahi, S. Roy, and A. Banerjee, "Controlled transportation of mesoscopic particles by enhanced spin-orbit interaction of light in an optical trap," *Phys. Rev. A*, vol. 87, 2013, Art. no. 043823.

[12] B. Roy, N. Ghosh, A. Banerjee, S. D. Gupta, and S. Roy, "Manifestations of geometric phase and enhanced spin Hall shifts in an optical trap," *New J. Phys.*, vol. 16, Art. no. 083037, 2014.

[13] A. Y. Bekshaev and M. Soskin, "Transverse energy flows in vectoral fields of paraxial beams with singularities," *Opt. Commun.*, vol. 271, no. 2, pp. 332–348, 2007.

[14] M.V. Berry, "Optical currents," *J. Opt. A: Pure Appl. Opt.*, vol. 11, 2009, Art. no. 094001.

[15] A. Y. Bekshaev, "Subwavelength particles in an inhomogeneous light field: Optical forces associated with the spin and orbital energy flows," *J. Opt.*, vol. 15, 2013, Art. no. 044004.

[16] K. Y. Bliokh, M. A. Alonso, E. A. Ostrovskaya, and A. Aiello, "Angular momenta and spin-orbit interaction of nonparaxial light in free space," *Phys. Rev. A*, vol. 82, 2010, Art. no. 063825.

[17] K. Y. Bliokh, A. Y. Bekshaev, and F. Nori, "Extraordinary momentum and spin in evanescent waves," *Nat. Commun.*, vol. 5, 2014, Art. no. 3300.

[18] J. S. Eismann, P. Banzer, and M. Neugebauer, "Spin-orbital coupling affecting the evolution of transverse spin," *Phys. Rev. Res.*, vol. 1, 2019, Art. no. 033143.

[19] P. B. Bareil and Y. Sheng, "Modeling highly focused laser beam in optical tweezers with the vector Gaussian beam in the T-matrix method," *J. Opt. Soc. Am. A*, vol. 30, pp. 1–6, 2013.

[20] F. G. Mitri, "Counterpropagating nondiffracting vortex beams with linear and angular momenta," *Phys. Rev. A*, vol. 88, 2013, Art. no. 035804.

[21] F.G. Mitri, "Quasi-Gaussian electromagnetic beams," *Phys. Rev. A*, vol. 87, 2013, Art. no. 035804.

[22] F. G. Mitri, "Vector spherical quasi-Gaussian vortex beams," *Phys. Rev. E*, vol. 89 2014, Art. no. 023205.

[23] P. L. Marston and J. H. Crichton, "Radiation torque on a sphere caused by a circularly-polarized electromagnetic wave," *Phys. Rev. A*, vol. 30, pp. 2508–2516, 1984.

[24] R. Hertel, "Theory of the inverse Faraday effect in metals," *J. Magn. Magnet. Mater.*, vol. 303, no. 1, pp. L1–L4, 2006.

[25] A. Ashkin and J. M. Dziedzic, "Optical levitation in high vacuum," *Appl. Phys. Lett.*, vol. 28, pp. 333–335, 1976.

[26] P. Meng, Z. Man, A. P. Konijnenberg, and H. P. Urbach, "Angular momentum properties of hybrid cylindrical vector vortex beams in tightly focused optical systems," *Opt. Express*, vol. 27, 2019, Art. no. 35336.

[27] S. Chang and S. S. Lee, "Optical torque exerted on a homogeneous sphere levitated in the circularly polarized fundamental-mode laser beam," *J. Opt. Soc. Am. B*, vol. 2, no. 11, pp. 1853–1860, 1985.

[28] V. V. Kotlyar, A. A. Kovalev, and A. G. Nalimov, "Energy density and energy flux in the focus of an optical vortex: Reverse flux of light energy," *Opt. Lett.*, vol. 43, no. 12, pp. 2921–2924, 2018.

[29] V. V. Kotlyar, S. S. Stafeev, and A. G. Nalimov, "Energy backflow in the focus of a light beam with phase or polarization singularity," *Phys. Rev. A.*, vol. 99, 2019, Art. no. 033840.

[30] K. Y. Bliokh, A. Y. Bekshaev, A. G. Kofman, and F. Nori, "Photon trajectories, anomalous velocities and weak measurements: A classical interpretation," *New J. Phys.*, vol. 15, 2013, Art. no. 073022.

[31] V. S. Ignatovsky, "Diffraction by a lens having arbitrary opening," *Trans. Opt. Inst. Petrograd*, vol. 1, 1919, Art. no. 4.

[32] M. A. Salem and H. Bagei, "Energy flow characteristics of vector X-waves," *Opt. Express*, vol. 19, pp. 8526–8532, 2011.

[33] P. Vaveliuk and O. Martinez-Matos, "Negative propagation effect in nonparaxial Airy beams," *Opt. Express*, vol. 20, pp. 26913–26921, 2012.

[34] F. G. Mitri, "Reverse propagation and negative angular momentum density flux of an optical nondiffracting nonparaxial fractional Bessel ortex beam of progressive waves," *J. Opt. Soc. Am. A*, vol. 33, no. 9, pp. 1661–1667, 2016.

[35] S. M. Barnett *et al.*, "On the natures of the spin and orbital parts of optical angular momentum," *J. Opt.*, vol. 18, 2016, Art. no. 064004.

[36] S. Saha, A. K. Singh, S. K. Ray, A. Banerjee, S. D. Gupta, and N. Ghosh, "Transverse spin and transverse momentum in scattering of plane waves," *Opt. Lett.*, vol. 41, no. 19, pp. 4499–4502, 2016.

[37] S. Zhang *et al.*, "Full controlled photonic spin in highly confined optical field," *Opt. Express*, vol. 27, no. 23, pp. 33621–33633, 2019.

[38] M. E. J. Friese, T. A. Nieminen, N. R. Heckenberg, and N. Rubinsztein-Dunlop, "Optical alignment and spinning of laser-trapped microscopic particles," *Nature*, vol. 394, pp. 348–350, 1998.

[39] S. M. Barnett, "Optical angular-momentum flux," *J. Opt. B: Quantum Semiclass. Opt.*, vol. 4, pp. S7–S16, 2002.

[40] A. Aiello, P. Banzer, M. Neugebauer, and G. Leuchs, "From transverse angular momentum to photonic wheels," *Nat. Photon.*, vol. 9, pp. 789–795, 2015.

[41] M. Li, Y. Cai, S. Yan, Y. Liang, P. Zhang, and B. Yao, "Orbit-induced localized spin angular momentum in strong focusing of optical vectorial vortex beams," *Phys. Rev. A*, vol. 97, 2018, Art. no. 053842.

[42] S. Sukhov and A. Dogariu, "On the concept of "tractor beams,"" *Opt. Lett.*, vol. 35, no. 22, pp. 3847–9, 2010.

[43] C. Rockstuhl and H. P. Herzig, "Calculation of the torque on dielectric elliptical cylinders," *Opt. Soc. Am. A.*, vol. 22, no. 1, pp. 109–116, 2005.

[44] F. G. Mitri, "Negative optical radiation force and spin torques on subwavelength prolate and oblate spheroids in fractional Bessel-Gauss pincers light-sheets," *J. Opt. Soc. Am A*, vol. 34, no. 7, pp. 1246–1254, 2017.

[45] The Classical Theory of Fields. Landau LD, Lifshitz EM. M.: Science, 1973. 504 p. ISBN 5-02-014420-7.

[46] M. Bethune-Waddell and K. J. Chau, "Simulation of radiation pressure experiments narrow down the energy and momentum of light in matter," *Rep. Prog. Phys.*, vol. 78, 2015, Art. no. 122401.

[47] A. Ashkin and J. M. Dziedzic„ "Radiation pressure on a free liquid surface," *Phys. Rev. Lett.*, vol. 30, no. 4, pp. 139–142, 1973.

[48] A. Ashkin, "Acceleration and trapping of particles by Radiation pressure," *Phys. Rev. Lett.*, vol. 24, no. 4, pp. 156–159, 1970.

[49] H. He, M. E. J. Friese, N. R. Heckenberg, and H. Rubinsztein-Dunlop, "Direct observation of transfer of angular momentum to absorptive particles from a laser beam with a phase singularity," *Phys. Rev. Lett.*, vol. 75, no. 5, pp. 826–829, 1995.